Excitation of soft dipole modes in electron scattering

C.A. Bertulani[1,2*]

[1] *Department of Physics and Astronomy University of Tennessee Knoxville, Tennessee 37996, USA*

[2] *Physics Division Oak Ridge National Laboratory P.O. Box 2008 Oak Ridge, Tennessee 37831, USAA*

Abstract

The excitation of soft dipole modes in light nuclei via inelastic electron scattering is investigated. I show that, under the proposed conditions of the forthcoming electron-ion colliders, the scattering cross sections have a direct relation to the scattering by real photons. The advantages of electron scattering over other electromagnetic probes is explored. The response functions for direct breakup are studied with few-body models. The dependence upon final state interactions is discussed. A comparison between direct breakup and collective models is performed. The results of this investigation are important for the planned electron-ion colliders at the GSI and RIKEN facilities.

PACS numbers: 25.30.Fj, 25.20.-x, 24.10.Nz

Keywords: Electron scattering, soft dipole modes, unstable nuclear beams.

*Electronic address: bertulanica@ornl.gov

I. INTRODUCTION

Reactions with radioactive beams have attracted great experimental and theoretical interest during the last two decades [1]. Progresses of this scientific adventure were reported on measurements of nuclear sizes [2], the use of secondary radioactive beams to obtain information on reactions of astrophysical interest [3, 4], fusion reactions with neutron-rich nuclei [5, 6], tests of fundamental interactions [7], dependence of the equation of state of nuclear matter upon the asymmetry energy [8], and many other research directions. Studies of the structure and stability of nuclei with extreme isospin values provide new insights into every aspect of the nuclear many-body problem. In neutron-rich nuclei far from the valley of β-stability, in particular, new shell structures occur as a result of the modification of the effective nuclear potential. Neutron density distributions become very diffuse and the phenomenon of the evolution of the neutron skin and, in some cases, the neutron halo have been observed.

New research areas with nuclei far from the stability line will become possible with newly proposed experimental facilities. Among these we quote the FAIR facility at the GSI laboratory in Germany. One of the projects for this new facility is the study of electron scattering off unstable nuclei in an electron-ion collider mode [9]. A similar proposal exists for the RIKEN laboratory facility in Japan [10]. By means of elastic electron scattering, these facilities will become the main tool to probe the charge distribution of unstable nuclei [11, 12]. This will complement studies of matter distribution which have been performed in other radioactive beam facilities using hadronic probes. Inelastic electron scattering will test the nuclear response to electromagnetic fields.

These facilities will provide accurate measurements of many nuclear properties of unstable nuclei. The reason is that electron scattering is a very clean probe. Its electromagnetic interaction with the nucleus is well understood. Inelastic electron scattering can also be very well described in the Born approximation. Higher order processes are only relevant for the distortion of the electron wavefunctions, affecting mostly electron scattering on heavy nuclei.

Up to now, the electromagnetic response of unstable nuclei far from the stability line has been studied with Coulomb excitation of radioactive beams impinging on a heavy target [4]. This method has been very useful in determining the electromagnetic response in light

nuclei [13]. For neutron-rich isotopes [14] the resulting photo-neutron cross sections are characterized by a pronounced concentration of low-lying $E1$ strength. The onset of low-lying $E1$ strength has been observed not only in exotic nuclei with a large neutron excess, but also in stable nuclei with moderate proton-neutron asymmetry. The problem with such experiments is that the probe is not very clean. It is well known that the nuclear interaction between projectile and target as well as the long range Coulomb distortion of the energy of the fragments interacting with the target (see, e.g. ref. [15]) are problems of a difficult nature. The nuclear response probed with electron does not suffer from these inconveniences.

The interpretation of the low-lying $E1$ strength in neutron-rich nuclei engendered a debate: are these "soft dipole modes" just a manifestation of the loosely-bound character of light neutron-rich nuclei, or are they a manifestation of the excitation of a resonance? [16, 17, 18, 19]. As far as I know, there has not been a definite answer to this simple question. This apparently innocuous question has nonetheless become the center of a even more widespread debate. It is believed that the weak binding of outermost neutrons gives rise to a direct break up of the nucleus and a consequent concentration of the electromagnetic response at low energies. The same weak binding can also lead to soft collective modes. In particular, the pygmy dipole resonance (PR), i.e. the resonant oscillation of the weakly-bound neutron mantle against the isospin saturated proton-neutron core. Its structure, however, remains very much under discussion. The electromagnetic response of light nuclei, leading to their dissociation, has a direct connection with the nuclear physics needed in several astrophysical sites [3, 4, 15]. In fact, it has been shown [20] that the existence of pygmy resonances have important implications on theoretical predictions of radiative neutron capture rates in the r-process nucleosynthesis, and consequently to the calculated elemental abundance distribution in the universe.

In this work I study the general features of inelastic electron scattering off light nuclei, in particular their response in the continuum. An assessment of the theory of inelastic electron scattering appropriate for the conditions of electron-ion colliders is presented in section 2. Special emphasis is put on the connection of electron scattering and the scattering by real photons, which will be useful to relate electron scattering and Coulomb dissociation measurements. Section 3 deals with the nuclear response within two and three-body models and their dependence upon final state interactions. Section 4 discusses the aspects of low energy collective modes in halo nuclei and their connection with the response obtained with

few-body models. The summary and conclusions will be presented in section 5.

II. INELASTIC ELECTRON SCATTERING

In the plane wave Born approximation (PWBA) the cross section for inelastic electron scattering is given by [21, 22]

$$\frac{d\sigma}{d\Omega} = \frac{8\pi e^2}{(\hbar c)^4}\left(\frac{p'}{p}\right)\sum_L \left\{ \frac{EE' + c^2\mathbf{p}\cdot\mathbf{p}' + m^2c^4}{q^4}\left|F_{ij}\left(q;CL\right)\right|^2 \right.$$
$$\left. + \frac{EE' - c^2\left(\mathbf{p}\cdot\mathbf{q}\right)\left(\mathbf{p}'\cdot\mathbf{q}\right) - m^2c^4}{c^2\left(q^2 - q_0^2\right)^2}\left[\left|F_{ij}\left(q;ML\right)\right|^2 + \left|F_{ij}\left(q;EL\right)\right|^2\right]\right\} \quad (1)$$

where J_i (J_f) is the initial (final) angular momentum of the nucleus, $(E, \mathbf{p})$ and $(E', \mathbf{p}')$ are the initial and final energy and momentum of the electron, and $(q_0, \mathbf{q}) = \left(\frac{(E-E')}{\hbar c}, \frac{(\mathbf{p}-\mathbf{p}')}{\hbar}\right)$ is the energy and momentum transfer in the reaction. $F_{ij}\left(q;\Pi L\right)$ are form factors for momentum transfer q and for Coulomb (C), electric (E) and magnetic (M) multipolarities, $\Pi = C, E, M$, respectively.

Here we will only treat electric multipole transitions. Moreover, we will treat low energy excitations such that $E, E' \gg \hbar c q_0$, which is a good approximation for electron energies $E \simeq 500$ MeV and small excitation energies $\Delta E = \hbar c q_0 \simeq 1 - 10$ MeV. These are typical values involved in the dissociation of nuclei far from the stability line.

Using the Siegert's theorem [23, 24], one can show that the Coulomb and electric form factors in eq. 1 are proportional to each other. Moreover, for very forward scattering angles ($\theta \ll 1$) the PWBA cross section, eq. 1, can be rewritten as

$$\frac{d\sigma}{d\Omega dE_\gamma} = \sum_L \frac{dN_e^{(EL)}\left(E, E_\gamma, \theta\right)}{d\Omega dE_\gamma}\ \sigma_\gamma^{(EL)}\left(E_\gamma\right), \quad (2)$$

where $\sigma_\gamma^{(EL)}\left(E_\gamma\right)$, with $E_\gamma = \hbar c q_0$, is the photo-nuclear cross section for the EL-multipolarity, given by [4]

$$\sigma_\gamma^{(EL)}\left(E_\gamma\right) = \frac{(2\pi)^3\left(L+1\right)}{L\left[(2L+1)!!\right]^2}\left(\frac{E_\gamma}{\hbar c}\right)^{2L-1}\frac{dB\left(EL\right)}{dE_\gamma}. \quad (3)$$

In the long-wavelength approximation, the response function, $dB\left(EL\right)/dE_\gamma$, in eq. 3 is given by

$$\frac{dB\left(EL\right)}{dE_\gamma} = \frac{\left|\left\langle J_f \left\| Y_L\left(\widehat{\mathbf{r}}\right)\right\| J_i\right\rangle\right|^2}{2J_i+1}\left[\int_0^\infty dr\ r^{2+L}\ \ \delta\rho_{if}^{(EL)}\left(r\right)\right]^2 w\left(E_\gamma\right), \quad (4)$$

where $w\left(E_\gamma\right)$ is the density of final states (for nuclear excitations into the continuum) with energy $E_\gamma = E_f - E_i$. The the transition density $\delta\rho_{if}^{(EL)}\left(r\right)$ will depend upon the nuclear model adopted.

For $L \geq 1$ one obtains from eq. (1) that

$$\frac{dN_e^{(EL)}\left(E, E_\gamma, \theta\right)}{d\Omega dE_\gamma} = \frac{4L}{L+1}\frac{\alpha}{E}\left[\frac{2E}{E_\gamma}\sin\left(\frac{\theta}{2}\right)\right]^{2L-1} \times \frac{\cos^2\left(\theta/2\right)\sin^{-3}\left(\theta/2\right)}{1+\left(2E/M_Ac^2\right)\sin^2\left(\theta/2\right)}\left[\frac{1}{2}+\left(\frac{2E}{E_\gamma}\right)^2\frac{L}{L+1}\sin^2\left(\frac{\theta}{2}\right)+\tan^2\left(\frac{\theta}{2}\right)\right]. \tag{5}$$

One can also define a differential cross section integrated over angles. Since $\sigma_\gamma^{(EL)}$ does not depend on the scattering angle, this can be obtained from eq. 5 by integrating $dN_e^{(EL)}/d\Omega dE_\gamma$ over angles, from $\theta_{\min} = E_\gamma/E$ to a maximum value θ_m, which depends upon the experimental setup.

Eqs. 2-5 show that under the conditions of the proposed electron-ion colliders, electron scattering will offer the same information as excitations induced by real photons. The reaction dynamics information is contained in the virtual photon spectrum of eq. 5, while the nuclear response dynamics information will be contained in eq. 4. This is akin to a method developed long time ago by Fermi [25] and usually known as the Weizsaecker-Williams method [26]. The quantities $dN_e^{(EL)}/d\Omega dE_\gamma$ can be interpreted as the number of equivalent (real) photons incident on the nucleus per unit scattering angle Ω and per unit photon energy E_γ. Note that $E0$ (monopole) transitions do not appear in this formalism. As immediately inferred from eq. 4, for $L = 0$ the response function $dB\left(EL\right)/dE_\gamma$ vanishes because the volume integral of the transition density also vanishes in the long-wavelength approximation. But for larger scattering angles the Coulomb multipole matrix elements (CL) in eq. 1 are in general larger than the electric (EL) multipoles, and monopole transitions become relevant [27].

In figure 1 we show the virtual photon spectrum for the $E1$, $E2$ and $E3$ multipolarities for electron scattering off arbitrary nuclei at $E_e = 100$ MeV. These spectra have been obtained assuming a maximum scattering angle of 5 degrees. An evident feature deduced from this figure is that the spectrum increases rapidly with decreasing energies. Also, at excitation energies of 1 MeV, the spectrum yields the ratios $dN_e^{(E2)}/dN_e^{(E1)} \simeq 500$ and

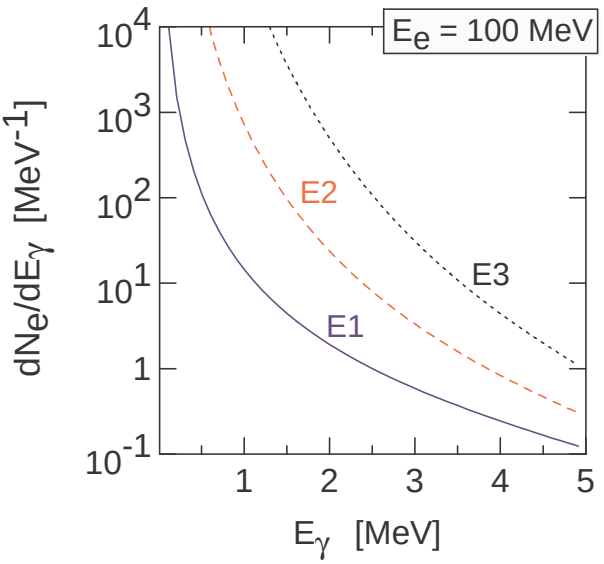

FIG. 1: (Color online) Virtual photon spectrum for the $E1$, $E2$ and $E3$ multipolarities in electron scattering off arbitrary nuclei at $E_e = 100$ MeV and maximum scattering angle of 5 degrees.

$dN_e^{(E3)}/dN_e^{(E2)} \simeq 100$. However, although $dN_e^{(EL)}/dE_\gamma$ increases with the multipolarity L, the nuclear response decreases rapidly with L, and $E1$ excitations tend to dominate the reaction. For larger electron energies the ratios $N^{(E2)}/N^{(E1)}$ and $N^{(E3)}/N^{(E1)}$ decrease rapidly.

Note that a similar relationship as eq. 2 also exists for Coulomb excitation [4] in heavy ion scattering. In figure 2 we show a comparison between the $E1$ virtual photon spectrum, dN_e/dE_γ, of 1 GeV electrons with the spectrum generated by 1 GeV/nucleon heavy ion projectiles. In the case of Coulomb excitation, the virtual photon spectrum was calculated in ref. [4], eq. 2.5.5a. For simplicity, we use for the strong interaction distance $R = 10$ fm. The spectrum for the heavy ion case is much larger than that of the electron for large projectile charges. For ^{208}Pb projectiles it can be of the order of 1000 times larger than that of an electron of the same energy. As a natural consequence, reaction rates for Coulomb excitation are larger than for electron excitation. But electrons have the advantage of being a clean electromagnetic probe, while Coulomb excitation at high energies needs a detailed theoretical analysis of the data due to contamination by nuclear excitation. As one observes in figure 2, the virtual spectrum for the electron contains more hard photons, i.e. the spectrum decreases slower with photon energy than the heavy ion photon spectrum. This is

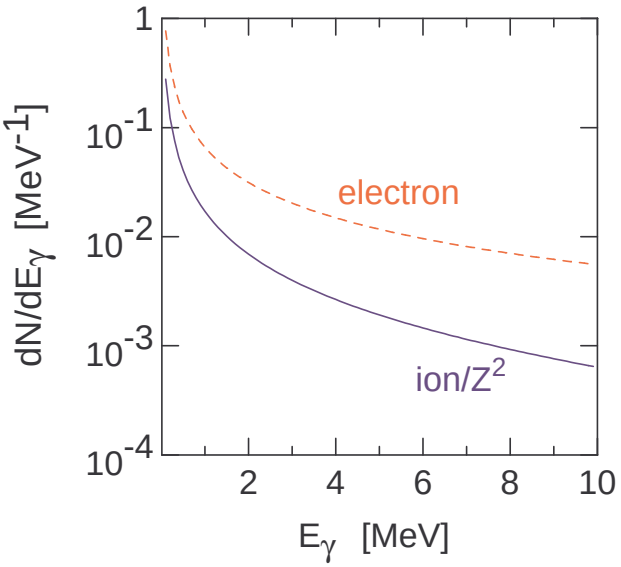

FIG. 2: (Color online) Comparison between the virtual photon spectrum of 1 GeV electrons (dashed line), and the spectrum generated by a 1 GeV/nucleon heavy ion projectile (solid line) for the $E1$ multipolarity, as a function of the photon energy. The virtual photon spectrum for the ion has been divided by the square of its charge number.

because, in both situations, the rate at which the spectrum decreases depends on the ratio of the projectile kinetic energy to its rest mass, E/mc^2, which is much larger for the electron ($m = m_e$) than for the heavy ion ($m =$ nuclear mass).

To obtain an effective luminosity per unit energy, the equivalent photon number is multiplied by the experimental luminosity, L_{eA}, i.e. $\frac{dL_{eff}}{dE_\gamma} = L_{eA}\frac{dN}{dE_\gamma}$. The number of events per unit time, N_τ, is given by the integral $N_\tau = \int \sigma(E_\gamma) dL_{eff}$, where $\sigma(E_\gamma)$ is the photonuclear cross section. Assuming that the photonuclear cross section peaks at energy E_0 and using the Thomas-Reiche-Kuhn (TRK) sum rule [1], we can approximate this integral by $N_\tau = \frac{dL_{eff}}{dE_0} \times 6 \times 10^{-26} \frac{NZ}{A}$, where dL_{eff}/dE is expressed in units of cm^{-2}s^{-1}MeV^{-1}. The giant resonances exhaust most part of the TRK sum rule and occur in nuclei at energies around $E_0 = 15$ MeV. For 1 GeV electrons $dN(E_\gamma = E_0)/dE_\gamma \approx 6 \times 10^{-3}$/MeV. With a luminosity of $L_{eA} = 10^{25}$ cm^{-2}s^{-1}, one gets $\frac{dL_{eff}}{dE_0} \approx 6 \times 10^{22}$ cm^{-2}MeV^{-1}s^{-1} and a number of events $N_\tau \approx 4 \times 10^{-3} NZ/A \approx 10^{-3} A$ s^{-1}. Thus, for medium mass nuclei, one expects thousands of events per day. These estimates increase linearly with the accelerator luminosity, L_{eA}, and show that studies of giant resonances in neutron-rich nuclei is very promising

at the proposed facilities [9, 10]. Only a small fraction, of the order of 5%-10%, of the TRK sum-rule goes into the excitation of soft-dipole modes [47]. However, these modes occur at a much lower energy, $E_r \approx 1$ MeV, where the number of equivalent photons (see figure 2) is at least one order of magnitude larger than for giant resonance energies. Therefore, inelastic processes leading to the excitation of soft dipole modes will be as abundant as those for excitation of giant resonances. However, one has to keep in mind that it is not clear if experiments with very short-lived nuclei will be feasible at the proposed electron-ion colliders.

III. DISSOCIATION OF WEAKLY-BOUND SYSTEMS

A. One-neutron halo

In this section I will consider the dissociation of a weakly-bound (halo) nucleus from a bound state into a structureless continuum. I calculate the matrix elements for the response function in eq. 4 with a two-body model which has been used previously to study Coulomb excitation of halo nuclei with relative success [29, 30, 31, 32, 33, 34]. The initial wavefunction can be written as $\Psi_{JM} = r^{-1} u_{ljJ}(r) \mathcal{Y}_{lJM}$, where $R_{ljJ}(r)$ is the radial wavefunction and $\mathcal{Y}_{lJM}$ is a spin-angle function [35]. The radial wavefunction, $u_{ljJ}(r)$, can be obtained by solving the radial Schrödinger equation for a nuclear potential, $V^{(N)}_{Jlj}(r)$. Some analytical insight may be obtained using a simple Yukawa form for an s-wave initial wavefunction, $u_0(r) = A_0 \exp(-\eta r)$, and a p-wave final wavefunction, $u_1(r) = j_1(kr)\cos\delta_1 - n_1(kr)\sin\delta_1$. In these equations η is related to the neutron separation energy $S_n = \hbar^2\eta^2/2\mu$, μ is the reduced mass of the neutron + core system, and $\hbar k = \sqrt{2\mu E_r}$, with E_r being the final energy of relative motion between the neutron and the core nucleus. A_0 is the normalization constant of the initial wavefunction. The transition density is given by $r^2 \delta\rho_{if}(r) = e_{eff} A_i u_i(r) u_f(r)$, where i and f indices include angular momentum dependence and $e_{eff} = -eZ_c/A$ is the effective charge of a neutron+core nucleus with charge Z_c. The $E1$ transition integral $\mathcal{I}_{l_i l_f} = \int_0^\infty dr\ r^3\ \ \delta\rho_{if}(r)$ for the wavefunctions described above yields

$$\begin{aligned}\mathcal{I}_{s\to p} &= e_{eff}\frac{2k^2}{\left(\eta^2+k^2\right)^2}\left[\cos\delta_1 + \sin\delta_1 \frac{\eta\left(\eta^2+3k^2\right)}{2k^3}\right] \\ &\simeq \frac{e_{eff}\hbar^2}{2\mu}\frac{2E_r}{\left(S_n+E_r\right)^2}\left[1+\left(\frac{\mu}{2\hbar^2}\right)^{3/2}\frac{\sqrt{S_n}\left(S_n+3E_r\right)}{-1/a_1+\mu r_1 E_r/\hbar^2}\right], \end{aligned} \tag{6}$$

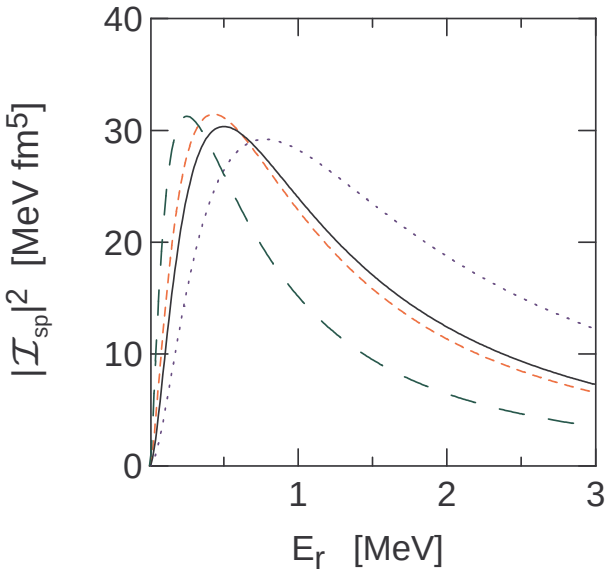

FIG. 3: (Color online) $|\mathcal{I}_{s\to p}|^2$ calculated using eq. 6, assuming $e_{eff} = e$, $A = 11$ and $S_n = 0.5$ MeV, as a function of E_r. The long dashed curve corresponds to $a_1 = -10$ fm^{-3} and $r_1 = -0.5$ fm^{-1}, the dashed curve corresponds to $a_1 = -50$ fm^{-3} and $r_1 = 1$ fm^{-1}, the solid curve corresponds to $a_1 = r_1 = 0$, and finally, the dotted curve corresponds to $a_1 = -10$ fm^{-3} and $r_1 = 0.5$ fm^{-1}.

where the effective range expansion of the phase shift, $k^{2l+1}\cot\delta \simeq -1/a_l + r_l k^2/2$, was used in the second line of the above equation. For $l = 1$, a_1 is the "scattering volume" (units of length^3) and r_1 is the "effective momentum" (units of 1/length). Their interpretation is not as simple as the $l = 0$ effective range parameters. Typical values are, e.g. $a_1 = -13.82$ fm^{-3} and $r_1 = -0.419$ fm^{-1} for n+^{4}He $p_{1/2}$-wave scattering and $a_1 = -62.95$ fm^{-3} and $r_1 = -0.882$ fm^{-1} for n+^{4}He $p_{3/2}$-wave scattering [36].

The energy dependence of eq. 6 has some unique features. As shown in previous works [29, 30, 37], the matrix elements for electromagnetic response of weakly-bound nuclei present a small peak at low energies, due to the proximity of the bound state to the continuum. This peak is manifest in the response function of eq. 4:

$$\frac{dB(EL)}{dE} \propto |\mathcal{I}_{s\to p}|^2 \propto \frac{E_r^{L+1/2}}{(S_n + E_r)^{2L+2}}. \tag{7}$$

It appears centered at the energy [30] $E_0^{(EL)} \simeq \frac{L+1/2}{L+3/2} S_n$ for a generic electric response of multipolarity L. For $E1$ excitations, the peak occurs at $E_0 \simeq 3S_n/5$.

The second term inside brackets in eq. 6 is a modification due to final state interactions.

This modification may become important, as shown in figure 3, where $|\mathcal{I}_{s\to p}|^2$ calculated with eq. 6 is plotted as a function of E_r. Here, for simplicity, I have assumed the values $e_{eff} = e$, $A = 11$ and $S_n = 0.5$ MeV. This does not correspond to any known nucleus and is used to assess the effect of the scattering length and effective range in the transition matrix element. The long dashed curve corresponds to $a_1 = -10$ fm^{-3} and $r_1 = -0.5$ fm^{-1}, the dashed curve corresponds to $a_1 = -50$ fm^{-3} and $r_1 = 1$ fm^{-1}, the solid curve corresponds to $a_1 = r_1 = 0$, and finally, the dotted curve corresponds to $a_1 = -10$ fm^{-3} and $r_1 = 0.5$ fm^{-1}. Although the effective range expansion is only valid for small values of E_r, it is evident from the figure that the matrix element is very sensitive to the effective range expansion parameters.

The strong dependence of the response function on the effective range expansion parameters makes it an ideal tool to study the scattering properties of light nuclei which are of interest for nuclear astrophysics. It is important to notice that the one-halo has been studied in many experiments, e.g. for the case of ^{11}Be for which there are many data available (see refs. [38, 39, 40]). In these papers one can find a detailed analysis of how the nuclear shell-model can explain the experimental data, by fitting the spectroscopic factors for several single-particle configurations. It is beyond the purpose of the present paper to reproduce theses data, in view of the simple model adopted above. The main goal of this section is to show the relevance of final state interactions.

B. Two-neutron halo

Many weakly-bound nuclei, like ^{6}He or ^{11}Li, require a three–body treatment in order to reproduce the electromagnetic response more accurately. In a popular three-body model, the bound–state wavefunction in the center of mass system is written as an expansion over hyperspherical harmonics (HH), see e.g. [41],

$$\Psi(\mathbf{x},\mathbf{y}) = \frac{1}{\rho^{5/2}} \sum_{KLSl_xl_y} \Phi^{l_xl_y}_{KLS}(\rho) \left[\mathcal{J}^{l_xl_y}_{KL}(\Omega_5) \otimes \chi_S\right]_{JM}. \tag{8}$$

Here $\mathbf{x}$ and $\mathbf{y}$ are Jacobi vectors where (see figure 4) $\mathbf{x} = \frac{1}{\sqrt{2}}(\mathbf{r}_1 - \mathbf{r}_2)$ and $y = \sqrt{\frac{2(A-2)}{A}}\left(\frac{\mathbf{r}_1+\mathbf{r}_2}{2} - \mathbf{r}_c\right)$, where A is the nuclear mass, $\mathbf{r}_1$ and $\mathbf{r}_2$ are the position of the nucleons, and $\mathbf{r}_c$ is the position of the core. The hyperradius ρ determines the size of a three-body state: $\rho^2 = x^2 + y^2$. The five angles $\{\Omega_5\}$ include usual angles (θ_x, ϕ_x), (θ_y, ϕ_y)

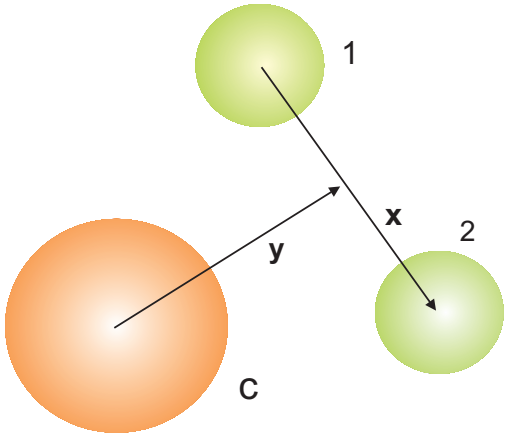

FIG. 4: (Color online) Jacobian coordinates ($\mathbf{x}$ and $\mathbf{y}$) for a three-body system consisting of a core (c) and two nucleons (1 and 2).

which parametrize the direction of the unit vectors $\widehat{\mathbf{x}}$ and $\widehat{\mathbf{y}}$ and the hyperangle θ, related by $x = \rho \sin\theta$ and $y = \rho \cos\theta$, where $0 \leq \theta \leq \pi/2$.

The insertion of the three-body wavefunction, eq. 8, into the Schrödinger equation yields a set of coupled differential equations for the hyperradial wavefunction $\Phi_{KLS}^{l_x l_y}(\rho)$. Assuming that the nuclear potentials between the three particles are known, this procedure yields the bound-state wavefunction for a three-body system with angular momentum J.

In order to calculate the electric response we need the scattering wavefunctions in the three-body model to calculate the integrals in eq. 4. One would have to use final wavefunctions with given momenta, including their angular information. When the final state interaction is disregarded these wavefunctions are three-body plane waves [43, 44]. To carry out the calculations, the plane waves can be expanded in products of hyperspherical harmonics in coordinate and momentum spaces. However, since we are only interested in the energy dependence of the response function, we do not need directions of the momenta. Thus, instead of using plane waves, I will use a set of final states which just include the coordinate space and energy dependence.

I will also adopt an approach closely related to the work of Pushkin et al. [43] (see also [45, 46]). For weakly-bound systems having no bound subsystems the hyperradial functions entering the expansion 8 behave asymptotically as [42] $\Phi_a(\rho) \longrightarrow \text{constant} \times \exp(-\eta\rho)$ as $\rho \longrightarrow \infty$, where the two-nucleon separation energy is related to η by $S_{2n} = \hbar^2\eta^2/(2m_N)$. This wavefunction has similarities with the two-body case, when ρ is interpreted as the

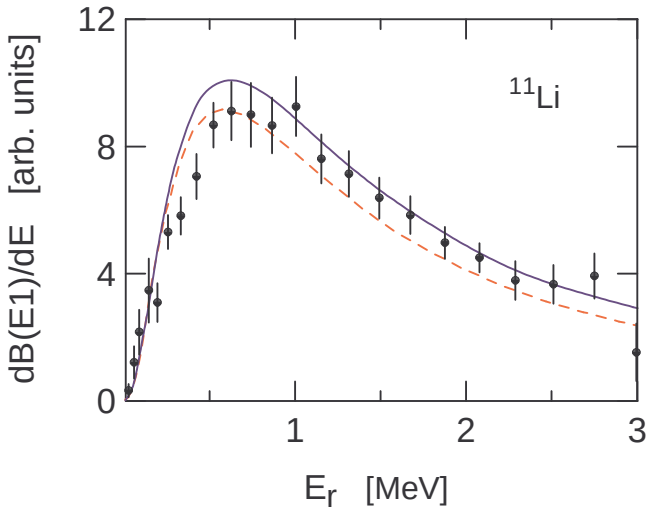

FIG. 5: (Color online) Comparison between the calculation of the response function (in arbitrary units) with eqs. 9 and 10, using $\delta_{nn} = 0$ and $\delta_{nc} = 0$, (dashed line), or including the effects of final state interactions (continuous line). The experimental data are from ref. [49].

distance r between the core and the two nucleons, treated as one single particle. But notice that the mass m_N would have to be replaced by $2m_N$ if a simple two-body (the dineutron-model [4, 37]) were used for ^{11}Li or ^{6}He.

Since only the core carries charge, in a three-body model the $E1$ transition operator is given by $M \sim yY_{1M}\left(\widehat{\mathbf{y}}\right)$ for the final state (see also [44]). The $E1$ transition matrix element is obtained by a sandwich of this operator between $\Phi_a\left(\rho\right)/\rho^{5/2}$ and scattering wavefunctions. In ref. [43] the scattering states were taken as plane waves. I will use distorted scattering states, leading to the expression

$$\mathcal{I}\left(E1\right) = \int dxdy \frac{\Phi_a\left(\rho\right)}{\rho^{5/2}}\, y^2 x u_p\left(y\right) u_q\left(x\right), \tag{9}$$

where $u_p\left(y\right) = j_1\left(py\right)\cos\delta_{nc} - n_1\left(py\right)\cos\delta_{nc}$ is the core-neutron asymptotic continuum wavefunction, assumed to be a p-wave, and $u_q\left(x\right) = j_0\left(qx\right)\cos\delta_{nn} - n_0\left(qx\right)\cos\delta_{nn}$ is the neutron-neutron asymptotic continuum wavefunction, assumed to be an s-wave. The relative momenta are given by $\mathbf{q} = \frac{1}{\sqrt{2}}\left(\mathbf{q}_1 - \mathbf{q}_2\right)$, and $\mathbf{p} = \sqrt{\frac{2(A-2)}{A}}\left(\frac{\mathbf{k}_1+\mathbf{k}_2}{2} - \mathbf{k}_c\right)$.

The $E1$ strength function is proportional to the square of the matrix element in eq. 9 integrated over all momentum variables, except for the total continuum energy $E_r =$

$\hbar^2 (q^2 + p^2) / 2m_N$. This procedure gives

$$\frac{dB(E1)}{dE_r} = \text{constant } \times \int |\mathcal{I}(E1)|^2 E_r^2 \cos^2\Theta \sin^2\Theta d\Theta d\Omega_q d\Omega_p, \tag{10}$$

where $\Theta = \tan^{-1}(q/p)$.

The $^1S_0$ phase shift in neutron-neutron scattering is remarkably well reproduced up to center of mass energy of order of 5 MeV by the first two terms in the effective-range expansion $k \cot \delta_{nn} \simeq -1/a_{nn} + r_{nn}k^2/2$. Experimentally these parameters are determined to be $a_{nn} = -23.7$ fm and $r_{nn} = 2.7$ fm. The extremely large (negative) value of the scattering length implies that there is a virtual bound state in this channel very near zero energy. The p-wave scattering in the n-^{9}Li (^{10}Li) system appears to have resonances at low energies [48]. I assume that this phase-shift can be described by the resonance relationsin $\delta_{nc} = (\Gamma/2)/\sqrt{(E_r - E_R)^2 + \Gamma^2/4}$, with $E_R = 0.53$ MeV and $\Gamma = 0.5$ MeV [48].

Most integrals in eqs. 9 and 10 can be done analytically, leaving two remaining integrals which can only be performed numerically. The result of the calculation is shown in figure 5. The dashed line was obtained using $\delta_{nn} = 0$ and $\delta_{nc} = 0$, that is, by neglecting final state interactions. The continuous curve includes the effects of final state interactions, with δ_{nn} and δ_{nc} parametrized as described above. The experimental data are from ref. [49]. The data and theoretical curves are given in arbitrary units. Although the experimental data is not perfectly described by either one of the results, it is clear that final state interactions are of extreme relevance.

As pointed out in ref. [43], the $E1$ three-body response function of ^{11}Li can still be described by an expression similar to eq. 7, but with different powers. Explicitly, $dB(E1)/dE_r \propto E_r^3 / \left(S_{2n}^{eff} + E_r\right)^{11/2}$. Instead of S_{2n}, one has to use an effective $S_{2n}^{eff} = aS_{2n}$, with $a \simeq 1.5$. With this approximation, the peak of the strength function in the three-body case is situated at about three times higher energy than for the two-body case, eq. 7. In the three-body model, the maximum is thus predicted at $E_0^{(E1)} \simeq 1.8 S_{2n}$, which fits the experimentally determined peak position for the ^{11}Li $E1$ strength function very well [43]. It is thus apparent that the effect of three-body configurations is to widen and to shift the strength function $dB(E1)/dE$ to higher energies.

It is worthwhile mentioning that the data presented in figure 5 and of other experiments [16, 50] is different in form and magnitude of the more recent experiment of Nakamura et al. [51]. The reason for the discrepancy is attributed to an enhanced sensitivity in the

experiment of ref. [51] to low relative energies below $E_{rel} = 0.5$ MeV compared to previous experiments. Also, this recent experiment agrees very well with the nn-correlated model of Esbensen and Bertsch [52]. This theoretical model is different than the model presented in this section in many aspects. In principle, the three-body models should be superior, as they include the interactions between the three-particles without any approximation. For example, ref. [52] use a simplified interaction between the two-neutrons. On the other hand, they include the many-body effects, e.g. the Pauli blocking of the occupied states in the core. It is not well known the reason why the data of ref. [51] is better described with the model of ref. [52] than traditional 3-body models.

IV. COLLECTIVE EXCITATIONS: THE PIGMY RESONANCE

A. The hydrodynamical model

We have seen that the energy position where the soft dipole response peaks depends upon the few body model adopted. Except for a two-body resonance in ^{10}Li, there was no reference to a resonance in the continuum. The peak in the response function can be simply explained by the fact that it has to grow from zero at low energies and return to zero at large energies. In few-body, or cluster, models, the form of the bound-state wavefunctions and the phase space in the continuum determine the position of the peak in the response function. Few-body resonances will lead to more peaks.

Now I shall consider the case in which a collective resonance is present. As with giant dipole resonances (GDR) in stable nuclei, one believes that pygmy resonances at energies close to the threshold are present in halo, or neutron-rich, nuclei. This was proposed by Suzuki et al. [53] using the hydrodynamical model for collective vibrations. The possibility to explain the soft dipole modes (figure 5) in terms of direct breakup, has made it very difficult to clearly identify the signature of pygmy resonances in light exotic nuclei.

The hydrodynamical model, first suggested by Goldhaber and Teller [54] and by Steinwedel and Jensen [55] needs adjustments to explain collective response in light, neutron-rich, nuclei. Because clusterization in light nuclei exists, not all neutrons and protons can be treated equally. The necessary modifications are straight-forward and discussed next. To my knowledge, the radial dependence of the transition densities in the hydrodynamical

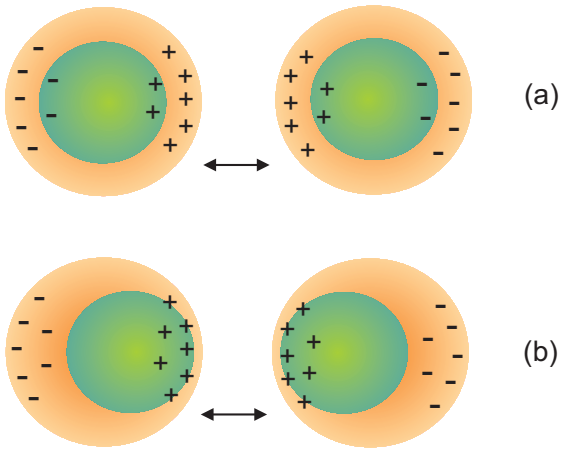

FIG. 6: (Color online) Hydrodynamical model for collective nuclear vibrations in halo nuclei. The (a) Steinwedel-Jensen (SJ) mode and the (b) Goldhaber-Teller (GT) mode are shown separately.

model for light, neutron-rich, nuclei has not been discussed in the literature. I will use the method of Myers et al. [56], who considered collective vibrations in nuclei as an admixture of Goldhaber-Teller and Steinwedel-Jensen modes.

When a collective vibration of protons against neutrons is present in a nucleus with charge (neutron) number Z (N), the neutron and proton fluids are displaced with respect to each other by $d_1 = \alpha_1 R$ and each of the fluids are displaced from the origin (center of mass of the system) by $d_p = Nd_1/A$ and $d_n = -Zd_1/A$. This leaves the center of mass fixed and one gets for the dipole moment $D_1 = Zed_p = \alpha_1 NZeR/A$. The GT model assumes that the restoring force is due to the increase of the nuclear surface which leads to an extra energy proportional to $A^{2/3}$. In this model, the inertia is proportional to A and the excitation energy is consequently given by $E_x \propto \sqrt{A^{2/3}/A} = A^{-1/6}$.

For light, weakly-bound nuclei, it is more appropriate to assume that the neutrons inside the core (A_c, Z_c) vibrate in phase with the protons. The neutrons and protons in the core are tightly bound. An overall displacement among them requires energies of the order of 10-20 MeV, well above that of the soft dipole modes. The dipole moment becomes $\mathbf{D}_1 = e\mathbf{d}_1(Z_cA - ZA_c)/A = Z^{(1)}_{eff} e\mathbf{d}_1$, where $\mathbf{d}_1$ is a vector connecting the center of mass of the two fluids (core and excess neutrons). We see that the dipole moment is now smaller than before because the effective charge changes from NZ/A in the case of the GDR to $Z^{(1)}_{eff} = (Z_cA - ZA_c)/A$. This effective charge is zero if $Z_cA = ZA_c$ and no pigmy resonance

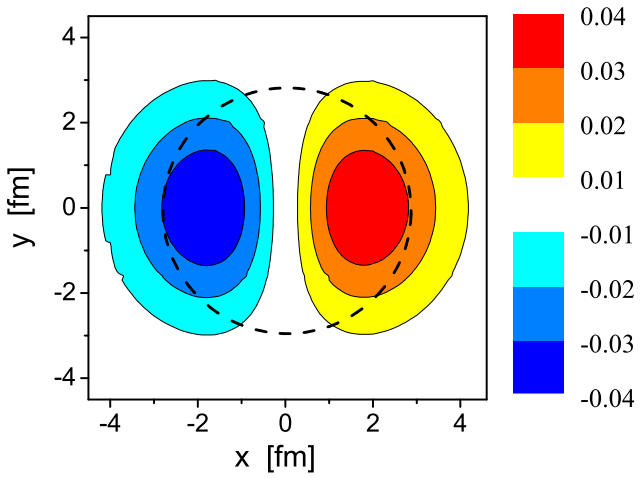

FIG. 7: (Color online) Contour plot of the nuclear transition density in the hydrodynamical model consisting of a mixture of GT and SJ vibrations. The darker areas represent the larger values of the transition density in a nucleus which has an average radius represented by the dashed circle. The legend on the right displays the values of the transition density within each contour limit.

is possible in this model, only the usual GDR.

Figure 6 shows a schematic representation of the hydrodynamical model for collective nuclear vibrations in a halo nucleus, as considered here. Part (a) of the figure shows the Steinwedel-Jensen (SJ) mode in which the total matter density of both the core and the halo nucleons do not change locally. Only the local ratio of the neutrons and protons changes. Part (b) of the figure shows a particular case of the Goldhaber-Teller (GT) mode, in which the core as a whole moves with respect to the halo nucleons.

For spherically symmetric densities, the transition density in the GT mode can be calculated from $\delta\rho_p = \rho_p\left(|\mathbf{r}-\mathbf{d}_p|\right) - \rho_p\left(\mathbf{r}\right)$, where ρ_p is the charge density. Using $d_1 \ll R$, it is straight-forward to show that $\delta\rho_p^{(1)}\left(\mathbf{r}\right) = \delta\rho_p^{(1)}\left(r\right) Y_{10}\left(\widehat{\mathbf{r}}\right)$, where

$$\delta\rho_p^{(1)}\left(r\right) = \sqrt{\frac{4\pi}{3}} Z_{eff}\alpha_1 R\frac{d\rho_0}{dr}, \tag{11}$$

and ρ_0 is the ground state matter density.

In the Steinwedel-Jensen (SJ) mode, the local variation of the density of protons is found

to be $\delta\rho_p^{(2)}(\mathbf{r}) = \delta\rho_p^{(2)}(r)\, Y_{10}(\widehat{\mathbf{r}})$, where

$$\delta\rho_p^{(2)}(r) = \sqrt{\frac{4\pi}{3}} Z_{eff}^{(2)} \alpha_2 K j_1(kr)\, \rho_0(r), \tag{12}$$

where $K = 9.93$. If the proton and neutron content of the core does not change [53], the effective charge number in the SJ mode is given by $Z_{eff}^{(2)} = Z^2(N - N_c)/A(Z + N_c)$.

The transition density at a point $\mathbf{r}$ from the center-of-mass of the nucleus is a combination of the SJ and GT distributions and is given by $\delta\rho_p(\mathbf{r}) = \delta\rho_p(r)\, Y_{10}(\widehat{\mathbf{r}})$, where

$$\delta\rho_p(r) = \sqrt{\frac{4\pi}{3}} R \left\{ Z_{eff}^{(1)} \alpha_1 \frac{d}{dr} + Z_{eff}^{(2)} \alpha_2 \frac{K}{R} j_1(kr) \right\} \rho_0(r). \tag{13}$$

Changes can be accommodated in these expressions to account for the different radii of the proton and neutron densities.

Figure 7 shows the contour plot, in arbitrary units, of the nuclear transition density in the hydrodynamical model, consisting of a mixture of GT and SJ vibrations. The darker areas represent the larger values of the transition density in a nucleus which has an average radius represented by the dashed circle. In this particular case, I have used the HF density [12, 57] for ^{11}Li, and a radius $R = 3.1$ fm. The parameters α_1 and α_2 were chosen so that $Z_{eff}^{(1)}\alpha_1 = Z_{eff}^{(2)}\alpha_2$, i.e. a symmetric mixture of the SJ and GT modes.

Figure 8 shows the transition densities for ^{11}Li for three different assumptions of the SJ+GT admixtures, according to eq. 13. The dashed curve is for a GT oscillation mode, with the core vibrating against the halo neutrons, with effective charge number $Z_{eff}^{(1)} = 6/11$, radius $R = 3.1$ fm, and $\alpha_1 = 1$. The dotted curve is for an SJ oscillation mode, with effective charge number $Z_{eff}^{(2)} = 2/11$, and $\alpha_2 = 1$. The solid curve is their sum. Notice that the transition densities are peaked at the surface, but at a radius smaller than the adopted "rms" radius $R = 3.1$ fm.

The liquid drop model predicts an equal admixture of SJ+GT oscillation modes for large nuclei [56]. The contribution of the SJ oscillation mode decreases with decreasing mass number, i.e. $\alpha_2 \longrightarrow 0$ as $A \longrightarrow 0$. This is even more probable in the case of halo nuclei, where a special type of GT mode (oscillations of the core against the halo nucleons) is likely to be dominant. For this special collective motion an approach different than those used in refs. [56] and [53] has to be considered. The resonance energy formula derived by Goldhaber and Teller [54] changes to

$$E_{PR} = \left(\frac{3\varphi\hbar^2}{2aRm_N A_r} \right)^{1/2}, \tag{14}$$

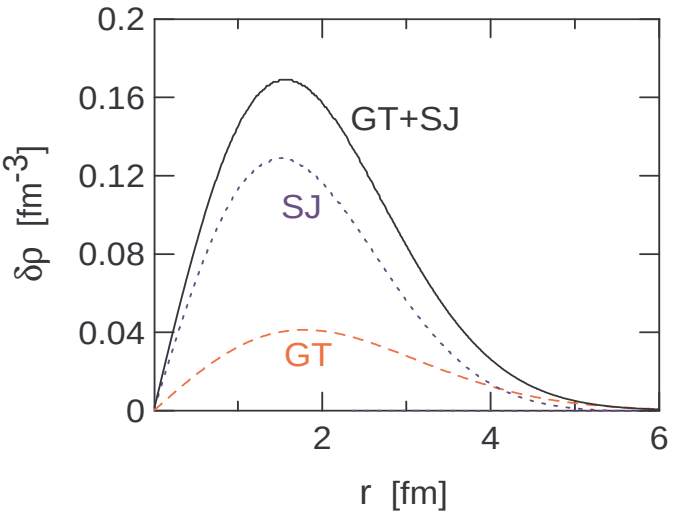

FIG. 8: (Color online) Hydrodynamical transition densities for ^{11}Li and three different assumptions for the SJ+GT admixtures, according to eq. 13. The dashed curve is for a GT oscillation mode, with the core vibrating against the halo neutrons, with effective charge number $Z^{(1)}_{eff} = 6/11$, radius $R = 3.1$ fm, and $\alpha_1 = 1$. The dotted curve is for an SJ oscillation mode, with effective charge number $Z^{(2)}_{eff} = 2/11$, and $\alpha_2 = 1$. The solid curve is their sum.

where $A_r = A_c\,(A - A_c)\,/A$ and a is the length within which the interaction between a neutron and a nucleus changes from a zero-value outside the nucleus to a high value inside, i.e. a is the size of the nuclear surface. φ is the energy needed to extract one neutron from the proton environment.

Goldhaber and Teller [54] argued that in a heavy stable nucleus φ is not the binding energy of the nucleus, but the part of the potential energy due to the neutron-proton interaction. It is proportional to the asymmetry energy. In the case of weakly-bound nuclei this picture changes and it is more reasonable to associate φ to the separation energy of the valence neutrons, S. I will use $\varphi = \beta S$, with a parameter β which is expected to be of order of one. Since for halo nuclei the product aR is proportional to S^{-1}, we obtain the proportionality $E_{PR} \propto S$. Using eq. 14 for ^{11}Li , with $a = 1$ fm, $R = 3$ fm and $\varphi = S_{2n} = 0.3$ MeV, we get $E_{PR} = 1.3$ MeV. Considering that the pygmy resonance will most probably decay by particle emission, one gets $E_r \simeq 1$ MeV for the kinetic energy of the fragments, which is within the right ballpark (see figure 5).

Both the direct dissociation model and the hydrodynamical model yield a bump in the

response function proportional to S, the valence nucleon(s) separation energy. In the direct dissociation model the width of the response function obviously depends on the separation energy. But it also depends on the nature of the model, i.e. if it is a two-body model, like the model often adopted for ^{11}Be or ^{8}B, or a three-body model, appropriate for ^{11}Li and ^{6}He. In the two-body model the phase-space depends on energy as $\rho\left(E\right) \propto d^3p/dE \propto \sqrt{E}$, while in the three-body model $\rho\left(E\right) \sim E^2$. This explains why the peak of figure 5 is pushed toward higher energy values, as compared to the prediction of eq. 7. It also explains the larger width of dB/dE obtained in three-body models. In the case of the pigmy resonance model, this question is completely open.

The hydrodynamical model predicts [56] for the width of the collective mode $\Gamma = \hbar\overline{\mathrm{v}}/R$, where $\overline{\mathrm{v}}$ is the average velocity of the nucleons inside the nucleus. This relation can be derived by assuming that the collective vibration is damped by the incoherent collisions of the nucleons with the walls of the nuclear potential well during the vibration cycles (piston model). Using $\overline{\mathrm{v}} = 3\mathrm{v}_F/4$, where $\mathrm{v}_F = \sqrt{2E_F/m_N}$ is the Fermi velocity, with $E_F = 35$ MeV and $R = 6$ fm, one gets $\Gamma \simeq 6$ MeV. This is the typical energy width a giant dipole resonance state in a heavy nucleus. In the case of neutron-rich light nuclei $\overline{\mathrm{v}}$ is not well defined. There are two average velocities: one for the nucleons in the core, $\overline{\mathrm{v}}_c$, and another for the nucleons in the skin, or halo, of the nucleus, $\overline{\mathrm{v}}_h$. One is thus tempted to use a substitution in the form $\overline{\mathrm{v}} = \sqrt{\overline{\mathrm{v}}_c\overline{\mathrm{v}}_h}$. Following ref. [58], the width of momentum distributions of core fragments in knockout reactions, σ_c, is related to the Fermi velocity of halo nucleons by $\mathrm{v}_F = \sqrt{5\sigma_c^2}/m_N$. Using this expression with $\sigma_c \simeq 20$ MeV/c, we get $\Gamma = 5$ MeV (with $R = 3$ fm). This value is also not in discordance with experiments (see figure 5).

Better microscopic models, e.g. those based on random phase approximation (RPA) calculations [59, 60] are necessary to study pigmy resonances. The halo nucleons have to be treated in an special way to get the response at the right energy position, and with approximately the right width [57, 60]. Electron scattering will provide a unique opportunity to clarify this issue due to its better resolution over Coulomb excitation.

B. Total inelastic cross sections

One might argue that the total breakup cross section would be a good signature for discerning direct dissociation versus the dissociation through the excitation of a pigmy collective

vibration. The trouble is that the energy weighted sum rule for both cases are approximately of the same magnitude [37, 53]. This can be shown by using the electric dipole strength function in the direct breakup model of ref. [37], namely

$$\frac{dB(E1)}{dE} = \mathcal{C}\frac{3\hbar e^2 Z_{eff}^2}{\pi^2 \mu}\frac{\sqrt{S_n}\,(E-S_n)^{3/2}}{E^4}, \tag{15}$$

where $E = E_r + S_n$ is the total excitation energy. $\mathcal{C}$ is a constant of the order of one, accounting for the corrections to the wavefunction used in ref. [37].

The sum rule for dipole excitations, $S_1\,(E1) = \int_{S_n}^{\infty} dE\ E\ \frac{dB(E1)}{dE}$, is

$$S_1\,(E1) = \mathcal{C}\left(\frac{9}{8\pi}\right)\frac{\hbar^2 e^2}{\mu} Z_{eff}^2, \tag{16}$$

with $Z_{eff}^2 = \left(Z_c A - Z A_c\right)^2 / [A A_c\,(A - A_c)]$. This is the same (with $\mathcal{C} = 1$) as eq. 1 of ref. [47], which is often quoted as the standard value to which models for the nuclear response in the region of pigmy resonance should be compared to. The response function in eq. 15, with $\mathcal{C} = 1$, therefore exhausts 100% of the so-called cluster sum rule [47]. The total cross section for electron breakup of weakly-bound systems is roughly proportional to S_1. This assertion can be easily verified by using eqs. 2 and 15, assuming that the logarithmic dependence of the virtual photon numbers on the energy $E \equiv E_\gamma$ can be factored out of the integral in eq. 2.

The dipole strength of the pigmy dipole resonance is given by the same equation 16. The constant $\mathcal{C}$ is still of the order of unity, but not necessarily the same as in eq. 15 and the effective charges are also different. For the Goldhaber-Teller pigmy dipole model the effective charge is given by $Z_{eff}^{(1)} = \left(Z_c A - Z A_c\right)/A$, whereas for the Steinwedel-Jensen it is $Z_{eff}^{(2)} = (Z^2/A)(N - N_c)/(Z + N_c)$. Assuming that the Goldhaber-Teller mode prevails, one gets the simple prediction for the ratio between the cross sections for direct breakup versus excitation of a pigmy collective mode:

$$\frac{\sigma^{direct}}{\sigma^{pigmy}} = \mathcal{C}\frac{A}{A_c\,(A - A_c)}. \tag{17}$$

For ^{11}Li this ratio is $11\mathcal{C}/18$ while for ^{11}Be it is $11\mathcal{C}/10$.

V. SUMMARY AND CONCLUSIONS

I have studied the feasibility to determine low energy excitation properties of light, exotic, nuclei from experimental data on inelastic electron scattering. It was shown that for the

conditions attained in the electron-ion collider mode, the electron scattering cross sections are directly proportional to photonuclear processes with real photons. This proportionality is lost when larger scattering angles, and larger ratio of the excitation energy to the electron energy, E_γ/E, are involved.

One of the important issues to be studied in future electron-ion colliders is the nuclear response at low energies. This response can be modeled in two ways: by a (a) direct breakup and by a (a) collective excitation. We have shown that in the case of direct breakup the response function will depend quite strongly on the final state interaction. This may become a very useful technique to obtain phase-shifts, or effective-range expansion parameters, of fragments far from the stability line. In the case of collective excitations, a variant of the Goldhaber-Teller and Steinwedel-Jensen model was used to obtain the transition densities in halo nuclei.

The pygmy resonance lies above the neutron emission threshold, effectively precluding its observation in (γ,γ') experiments on very neutron-rich nuclei. Nonetheless, electron scattering experiments will probe the response function under several conditions, including different bombarding energies, different scattering angles, etc. The study of pygmy resonances and of final state interactions will certainly be an important line of investigation in these facilities.

Acknowledgments

The author is grateful to Haik Simon and Toshimi Suda for useful discussions. This work was supported by the U. S. Department of Energy under grant No. DE-FG02-04ER41338.

---

[1] C.A. Bertulani, M.S. Hussein, and G. Münzenberg, *Physics of Radioactive Beams* (Nova Science Publishers, Hauppage, NY, 2002).

[2] I. Tanihata et al., Phys. Rev. Lett. **55** (1985) 2676.

[3] G.Baur, C.A.Bertulani and H.Rebel, Nucl. Phys. **A458** (1986) 188.

[4] C.A.Bertulani and G.Baur, Phys. Reports **163** (1988) 299.

[5] N. Takigawa and H. Sagawa, Phys. Lett. **B 265** (1991) 23.

[6] M. S. Hussein et al., Phys. Rev. **C 46** (1992) 377.

[7] J. Hardy, in *Physics of Unstable Nuclear Beams*, Edited by C.A.Bertulani et al., World Scientific, Singapore, 1997.

[8] P. Danielewicz, R. Lacey and W. G. Lynch, Science **298**, 1592 (2002).

[9] Haik Simon, *Technical Proposal for the Design, Construction, Commissioning, and Operation of the ELISe setup*, GSI Internal Report, Dec. 2005.

[10] T. Suda, K. Maruayama, *Proposal for the RIKEN beam factory*, RIKEN, 2001; M. Wakasugia, T. Suda, Y. Yano, Nucl. Inst. Meth. Phys. **A 532**, 216 (2004).

[11] A.N. Antonov et al., Phys. Rev. **C72**, 044307 (2005).

[12] C.A. Bertulani, Los Alamos archive, nucl-th/0604044.

[13] C.A. Bertulani, L.F. Canto and M.S. Hussein, Phys. Reports **226**(1993) 281.

[14] A. Leistenschneider et al., Phys. Rev. Lett. **86,** 5442 (2001).

[15] C.A.Bertulani, Phys. Rev. Lett. **94**, 072701 (2005).

[16] K. Ieki et al., Phys. Rev. Lett. **70,** 730 (1993).

[17] D. Sackett et al., Phys. Rev. **C 48**, 118 (1993).

[18] H. Sagawa et al., Z. Phys. **A 351**, 385 (1995).

[19] M.S. Hussein, C.Y Lin and A.F.R. de Toledo Piza, Z. Phys. **A 355** (1966) 165.

[20] S. Goriely, Phys. Lett. **B 436** (1998) 10.

[21] W.C. Barber, Ann. Rev. Nucl. Sci. **12**, 1 (1962).

[22] J.M. Eisenberg and W. Greiner, "Excitation Mechanisms of the Nucleus", (North-Holland, Amsterdam, 1988).

[23] A.J.F. Siegert, Phys. Rev. **52**, 787 (1937).

[24] R.G. Sachs and N. Austern, Phys. Rev. **81**, 705 (1951).

[25] E. Fermi, Z. Physik **29,** 315 (1924).

[26] C.F. Weizsaecker,. Z. Physik **88**, 612 (1934);, E.J. Williams, Phys. Rev. **45**, 729 (1934).

[27] L.I. Schiff, Phys. Rev. **96**, 765 (1954).

[28] J.M. Eisenberg, Phys. Rev. **132,** 2243 (1963).

[29] C.A. Bertulani and G. Baur, Nucl. Phys. **A480**, 615 (1988).

[30] C.A. Bertulani and A. Sustich, Phys. Rev. **C 46**, 2340 (1992).

[31] T. Otsuka et al., Phys. Rev. **C 49**, R2289 (1994).

[32] A. Mengoni, T. Otsuka and M. Ishihara, Phys. Rev. C **52**, R2334 (1995).

[33] D.M. Kalassa and G. Baur, J. Phys. **G 22**, 115 (1996).

[34] S. Typel and G. Baur, Phys. Rev. Lett. **93**, 142502 (2004).

[35] C.A. Bertulani and P. Danielewicz, *Introduction to Nuclear Reactions* (IOP Publishing, Bristol, UK, 2004).

[36] R.A. Arndt, D.L. Long, L.D. Roper, Nucl. Phys. **A209** (1973) 429.

[37] C. A. Bertulani, G. Baur and M. S. Hussein, Nucl. Phys. **A 526** (1991) 751.

[38] T. Nakamura et al., Phys. Lett. **B331**, 296 (1994).

[39] R. Palit et al., Phys. Rev. **C68**, 034318 (2003).

[40] N. Fukuda et al., Phys. Rev. **C70**, 054606 (2004).

[41] M. V. Zhukov, B.V. Danilin, D.V. Fedorov, J.M. Bang, I.J. Thompson and J.S. Vaagen, Phys. Rep. **231**, 151 (1993).

[42] S.P. Merkuriev, Sov. J. Nucl. Phys. **19** (1974) 222.

[43] A Pushkin, B Jonson and M V Zhukov, J. Phys. **G 22** (1996) L95.

[44] L.V. Chulkov, B. Jonson and M.V. Zhukov, J. Phys. **G 22** (1996) 95.

[45] C. Forssen, V.D. Efros and M.V. Zhukov, Nucl. Phys. **A 697** (2002) 639.

[46] C. Forssen, V.D. Efros and M.V. Zhukov, Nucl. Phys. **A 706** (2002) 48.

[47] Y. Alhassid, M. Gai and G.F. Bertsch, Phys. Rev. Lett. **49** (1982) 1482.

[48] M. Thoennessen et al., Phys. Rev. **C 59**, 111 (1999).

[49] S. Shimoura et al., Phys. Lett. **B 348** (1995) 29.

[50] M. Zinser et al., Nucl. Phys. **A619**, 151 (1997).

[51] T. Nakamura et al., Phys. Rev. Lett. **96**, 252502 (2006).

[52] H. Esbensen and G. F. Bertsch, Nucl. Phys. **A542**, 310 (1992).

[53] Y. Suzuki, K. Ikeda, and H. Sato, Prog. Theor. Phys. **83**, 180 (1990).

[54] M. Goldhaber and E. Teller, Phys. Rev. **74**, 1046 (1948).

[55] H. Steinwedel and H. Jensen, Z. Naturforschung **5A**, 413 (1950).

[56] W.D. Myers, W.G. Swiatecki, T. Kodama, L.J. El-Jaick and E.R. Hilf, Phys. Rev. **C 15,** 2032 (1977).

[57] H. Sagawa and C.A. Bertulani, Prog. Theo. Phys. Suppl. **124**, 143 (1996).

[58] C.A. Bertulani and K.W. McVoy, Phys. Rev. **C48** (1993) 2534.

[59] G.F. Bertsch and J. Foxwell, Phys. Rev. **C41** (1990) 1300.

[60] N. Teruya, C.A. Bertulani, S. Krewald, H. Dias, and M.S. Hussein, Phys. Rev. **C43** (1991) R2049.